搅拌针形状影响搅拌摩擦焊过程金属塑性流动规律的数值模拟

姬书得[1]， 孟庆国[3]， 史清宇[2]， 张利国[1]， 邹爱丽[1]
(1. 沈阳航空航天大学 航空航天工程学部，沈阳 110136; 2. 清华大学 机械工程系，北京 100084;
3. 南通中集罐式储运设备制造有限公司，南通 226001)

摘 要: 考虑材料参数随温度的变化关系以及搅拌工具的实际结构，利用 Fluent 流体力学软件建立了搅拌摩擦焊的有限体积模型，对搅拌针的形状影响材料塑性流动行为的规律进行了研究. 结果表明，材料的流动速度随着到焊件表面以及到搅拌针旋转轴的距离增加而减小; 当减小搅拌针的锥角以及减小搅拌针的螺纹槽宽度时，焊件内部材料的流动速度得到提高. 当搅拌工具在焊接过程中顺时针旋转时，对于左螺旋搅拌针，搅拌针附近的材料向下流动，而热力影响区材料的流动方向向上，此规律与右螺旋搅拌针时相反.

关键词: 搅拌摩擦焊; 流动; 搅拌针; 数值模拟
中图分类号: TG453 **文献标识码**: A **文章编号**: 0253－360X(2013)02－0093－04

姬书得

0 序 言

作为一种新型的固相连接技术，搅拌摩擦焊(friction stir welding，FSW)具有低应力、无变形、接头强度高、无常规熔焊缺陷以及绿色无污染等优点. 由于不存在金属熔化现象，搅拌摩擦焊过程中塑性金属材料的流动决定了接头质量的优劣[1,2]. 因此搅拌摩擦焊焊缝金属的塑性流动行为始终是国内外科研工作者的研究热点.

尽管研究搅拌摩擦焊塑性金属流动行为的试验方法很多，但其很难得到焊核区域金属材料的流动轨迹[3-5]. 因此利用数值模拟的方法研究搅拌摩擦焊塑性金属的流动行为成为了一种趋势[6,7]. Zhang 等人[8]利用有限元软件 Deform 研究了搅拌头端面结构形状影响焊缝及其附近区域塑性金属流动行为的规律. Colegrove 等人[9]利用 CFD 软件 Fluent 研究了焊接工艺参数影响搅拌摩擦焊焊缝中塑性金属流动的规律.

组成搅拌工具的搅拌针是影响焊接过程中材料流动的关键因素. 科研工作者对于搅拌针影响接头材料流动、性能等方面开展了大量的研究[10,11]，但目前未见利用数值模拟的方法研究搅拌针形状参数影响搅拌摩擦焊过程材料流动行为的相关报道. 鉴于此，文中利用 Fluent 软件中的有限体积法研究焊接过程中金属材料塑性流动行为，探讨组成搅拌工具的搅拌针形状参数对塑性材料流动速度的影响规律. 此研究对于搅拌摩擦焊的焊接工艺优化以及搅拌工具形状优化提供了技术支持.

收稿日期: 2011－12－20

1 搅拌摩擦焊的流场模型

1.1 实体模型与网格划分

适用于铝合金搅拌摩擦焊的搅拌工具主要有两部分组成: 轴肩与搅拌针(图1). 其中轴肩结构为内凹，其直径为 14 mm; 搅拌针上的螺纹旋向为右旋，其长度取 5.3 mm，且根部与端部直径分别为 5.5 mm 与 3 mm. 试板的尺寸取 150 mm × 50 mm × 6.5 mm. 模拟用流场模型的网格划分情况如图2所示.

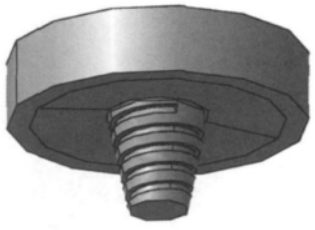

图1 搅拌工具的实体模型

Fig. 1 Solid model of rotational tool

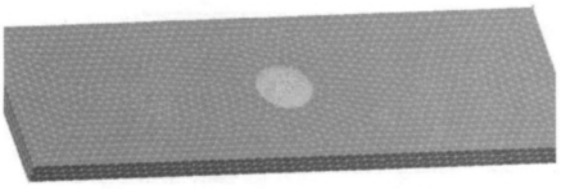

图 2 模拟用模型的网格划分情况

Fig. 2 Mesh generation of model

1.2 边界条件的设置

在模拟过程中，金属材料视为流体且绕过旋转的搅拌针，采用欧拉流动公式进行计算. 将焊件上表面、下表面、流体流动入口及出口、前进侧和回退侧均设为移动墙，移动速度与焊接速度(100 mm/min)相同，移动方向与焊接方向相反. 轴肩端面与搅拌针侧面定义为旋转墙，旋转方向与搅拌工具旋转方向相同，即顺时针旋转; 旋转频率与搅拌工具的旋转频率相同，即 800 r/min.

根据搅拌摩擦焊温度场的分布特点，取搅拌头区域的温度峰值为材料熔点的 80%，约 400 ℃，并加载到旋转边界上，采用热 - 流耦合方法进行计算.

1.3 材料参数的确定

对于基于欧拉方程的流场模型来讲，材料参数主要涉及 3 个: 比热、热导率与粘性系数. 此模型考虑了材料参数随温度之间的变化关系，如表 1 所示.

表 1 2024 铝合金的材料参数

Table 1 Material parameters of 2024 Al alloy

温度 T/℃	比热 C/(J·kg^{-1}·℃$^{-1}$)	热导率 K/(W·m^{-1}·℃$^{-1}$)
25	921	122
100	921	134
200	1 047	151
300	1 130	172
400	1 172	176

模型中考虑了材料的粘度与温度及应变速率之间的关系[12]，即

$$\eta=\frac{1}{3\bar{\varepsilon}\alpha}\ln\left\{\left(\frac{Z(T,\bar{\varepsilon})}{A}\right)^{-\frac{1}{n}}+\left[1+\left(\frac{Z(T,\bar{\varepsilon})}{A}\right)^{\frac{2}{n}}\right]^{\frac{1}{2}}\right\} \tag{1}$$

$$Z(T,\bar{\varepsilon})=\bar{\varepsilon}\exp\left(\frac{Q}{RT}\right) \tag{2}$$

式中: η 为粘度; T 为温度; $\bar{\varepsilon}$ 为应变速率; Q 为激活能，其值为 176 876 J/mol; R 为普适气体常数，其值为 8.314 J/mol·K; α，A 与 n 为材料有关的常数，其值如下: $\alpha=0.016/\mathrm{MPa}$，$\ln A=19.6/\mathrm{s}$，$n=4.27$.

2 结果与讨论

为了研究搅拌摩擦焊过程的流场分布规律，取不同位置的截面进行了分析. 截面位置示意图如图 3 所示，其中截面 a、截面 b 与截面 c 均与焊件表面平行，且截面 a 与截面 b 到轴肩端面的距离分别为 0.1 mm 与 4 mm，截面 c 到搅拌针端面的距离为 0.1 mm. 同时文中也对经过搅拌针旋转轴且沿垂直焊接方向的截面进行了分析.

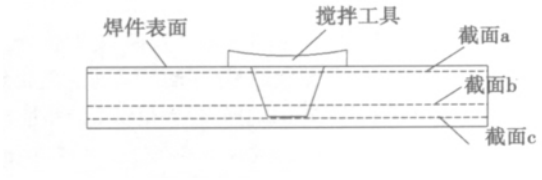

图 3 不同截面的位置示意图

Fig. 3 Position of different sections

2.1 三维流场

图 4 为搅拌摩擦焊过程中材料在水平方向的流动速度矢量图.

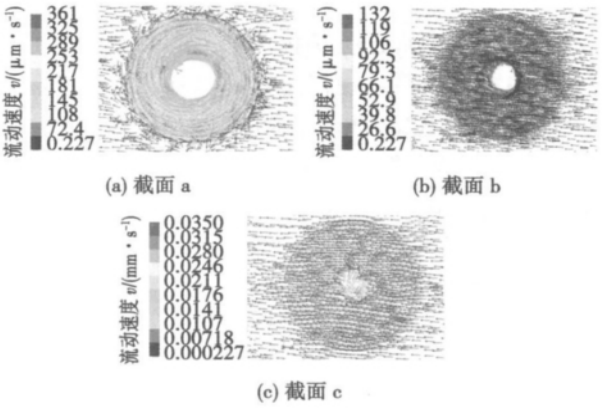

图 4 搅拌摩擦焊过程中沿水平方向上不同截面的材料流动

Fig. 4 Material flow velocity of different sections parallel to weldment surface during FSW

通过分析可知，搅拌针及其附近区域的材料流动方向与搅拌工具的旋转方向一致; 在垂直焊件表面的方向上，材料的流动速度随到焊件表面距离的增加而逐渐减小，且高速流动区的范围随搅拌针的直径变化而变化. 在平行焊件表面方向上，与轴肩以及搅拌针接触区域的材料流动速度远大于其它区域; 在搅拌工具与焊件间作用力以及搅拌区材料高速流动的作用下塑性变形区大于轴肩直径或搅拌针直径. 同时在搅拌针端面与焊件底面的区域，材料

的塑性金属流动不充分,这也是缺陷最容易出现的位置.

2.2　螺纹槽大小对流场的影响

为了研究螺纹槽的变化对材料流动的影响,建立了如图 5 所示的宽螺纹槽搅拌工具. 与图 1 所示的搅拌工具相比,图 5 中搅拌工具除螺纹槽较宽之外,其它结构与尺寸均相同(如轴肩直径等) .

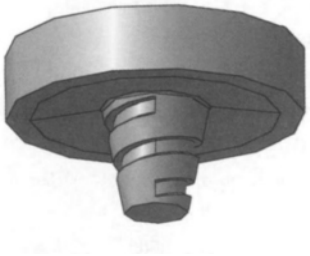

图 5　宽螺纹槽的搅拌工具实体模型

Fig. 5　Solid model of rotational tool with big pitch of screws

图 6 为采用宽螺纹槽的搅拌工具时材料在水平方向的流动速度矢量图. 结合图 4 可知,在搅拌针的螺纹区域,宽螺纹槽的搅拌工具情况下材料在相同位置的流动速度小于窄螺纹槽搅拌工具的情况,这一现象可用流体流动的连续性定理解释. 由于高速旋转的材料可以看作是不可压缩的流体,根据连续性定理可知,在同一时间内,流过螺纹槽任意截面的材料质量都是相等的. 那么则有

$$v_1 A_1 = v_2 A_2 = \text{常数} \tag{3}$$

式中: v 为材料的流动速度; A 为螺纹槽截面面积; 下标 1 与 2 分别表示不同的截面. 当搅拌针上的螺纹槽变大时,即 A 变大,造成 v 变小,即材料的流动速度变小. 这就说明了宽螺纹槽搅拌针的材料流速低于窄螺纹槽搅拌针的原因.

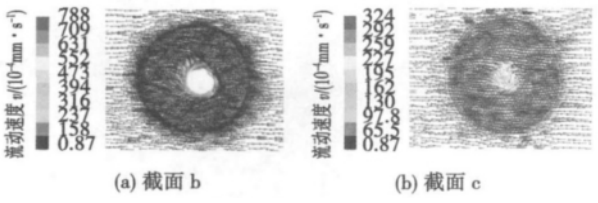

图 6　宽螺纹槽搅拌针情况下的材料流动速度矢量图

Fig. 6　Material flow velocity of different sections under condition of big pitch of screws

2.3　搅拌针锥角对流场的影响

为了比较搅拌针的锥角变化对材料流动的影响,设计了一个大锥角搅拌针的搅拌工具,如图 7 所示. 图 8 为大锥角搅拌针情况下材料在不同截面上的流动速度矢量图. 结合图 4 的模拟结果可知,增加搅拌针的锥角会降低与搅拌针接触区域材料流动速度,甚至造成搅拌针端部下方的材料流动速度趋近于 0,易于形成根部缺陷. 事实上,焊接过程中的热量主要由摩擦热以及塑性变形热两部分组成,采用较大锥角的搅拌针(如圆柱形等) 时会导致焊核区的温度升高[13],使热影响区变宽,不利于接头性能. 因此搅拌工具的搅拌针锥角要适中,太小与太大都不好.

图 7　大锥角的搅拌工具实体模型

Fig. 7　Solid model of rotational tool with small cone angle

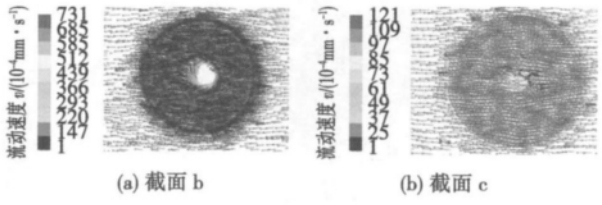

图 8　大锥角搅拌针情况下的材料流动速度矢量图

Fig. 8　Material flow velocity of different sections under the condition of big cone angle

2.4　螺旋方向对流场的影响

为了比较螺纹旋向对搅拌工具及其附近区域的材料流动的影响规律,对比分析了螺旋方向分别是左旋与右旋的情况. 模拟用左螺旋搅拌针的搅拌工具的实体结构如图 9 所示.

图 9　左螺旋搅拌针的搅拌工具实体模型

Fig. 9　Solid model of rotational tool with left screw

图 10 为搅拌针的螺纹旋向不同时材料的流动情况. 为了便于观察,图 10 中的流动矢量忽略了沿 x 方向的速度. 通过分析可知,改变螺纹旋向对于焊缝表面、焊件内部等区域的材料流动速率几乎没有影响,但材料的流动方向却发生根本性的变化. 对于右螺旋来讲,位于搅拌针表面及附近的大部分材料随着搅拌针的旋转向上流动,而位于热力影响区及其附近区域的材料的流动方向为向下; 对于左螺旋来说,位于搅拌针表面及附近的大部分材料随着搅拌针的旋转向下流动,而位于热力影响区及其附近区域的材料的流动方向为向上. 此模拟结果已被相应的试验结果所证实[11].

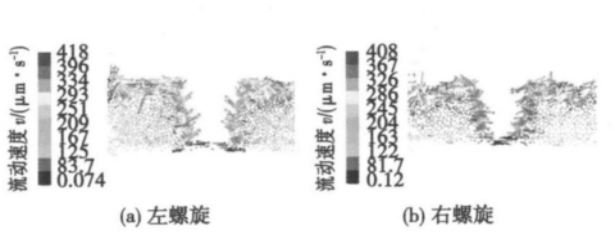

图 10 螺旋方向对材料流动方向的影响规律

Fig. 10 Effect of spiral direction on direction of material flow

3 结 论

(1) 在搅拌摩擦焊过程中,材料的流动速度随着到焊件表面距离的增加而减小,随着到搅拌针旋转轴距离的增加而减小. 当搅拌工具顺时针旋转且搅拌针上的螺纹为左旋时,位于搅拌针表面及附近的大部分材料向下流动,位于热力影响区及其附近区域材料的流动方向向上; 当搅拌工具顺时针旋转且针上的螺纹为右旋时,材料流动方向与左旋时相反.

(2) 减小搅拌针的螺纹槽大小以及减小搅拌针的锥角有利于提高焊件内部材料在焊接过程中的流动速度,避免根部缺陷的发生.

参考文献:

[1] 赵衍华, 林三宝, 吴 林. 2014 铝合金搅拌摩擦焊接过程塑性金属流变可视化[J]. 焊接学报, 2005, 26(6): 73 - 75.
Zhao Yanhua, Lin Sanbao, Wu Lin. Visualization of the plastic material flow in friction stir welding of 2024 aluminum alloy [J]. Transactions of the China Welding Institute, 2005, 26(6): 73 - 75.

[2] Nandan R, Roy G G, Lienert T J, *et al*. Three-dimensional heat and material flow during friction stir welding of mild steel [J]. Acta Materialia, 2007, 55: 883 - 895.

[3] Colligan K. Material flow behavior during friction stir welding of aluminum [J]. Welding Journal, 1999, 78(2): 229 - 237.

[4] Fonda R W, Bingert J F, Colligan K J. Development of grain structure during friction stir welding [J]. Scripta Materialia, 2004, 51(3): 2879 - 2884.

[5] Seidel T U, Reynolds A P. Visualization of the material flow in AA2195 friction stir welding using a marker insert technique [J]. Metallurgical and Materials Transactions A, 2001, 32(11): 2879 - 2884.

[6] Zhang H W, Zhang Z, Chen J T. The finite element simulation of the friction stir welding process [J]. Materials Science and Engineering A, 2005, 43: 340 - 348.

[7] Buffa G, Hua J, Shivpuri R, *et al*. A continuum based fem model for friction stir welding-model development [J]. Materials Science and Engineering A, 2006, 419: 389 - 396.

[8] Zhang Liguo, Ji Shude, Luan Guohong, *et al*. Friction stir welding of thin plate of Al alloy by rotational tool without pin [J]. Journal Material Science & Technology, 2011, 27(7): 647 - 652.

[9] Colegrove P A, Shercliff H R. 3-Dimensional CFD modeling of flow round a threaded friction stir welding tool profile [J]. Journal of Materials Processing Technology, 2005, 169: 320 - 327.

[10] 张 昭, 刘会杰. 搅拌头形状对搅拌摩擦焊材料变形和温度场的影响[J]. 焊接学报, 2011, 32(3): 5 - 8.
Zhang Zhao, Liu Huijie. Effect of pin shapes on material deformation and temperature filed in friction stir welding [J]. Transactions of the China Welding Institute, 2011, 32(3): 5 - 8.

[11] 王善林, 柯黎明, 邢 丽. 搅拌头形状对焊缝塑性金属流动行为的影响[J]. 南昌航空工业学院学报: 自然科学版, 2005, 19(1): 62 - 66.
Wang Shanlin, Ke Liming, Xing Li. The influence of pin shape on the flow behavior of the plasticized metal in the weld during the friction stir welding [J]. Journal of Nanchang Institute of Aeronautical Technology(Natural Sceince), 2005, 19(1): 62 - 66.

[12] Sheppard A, Jackson A. Constitutive equation for use in prediction of flow stress duringextrusion of aluminum alloy [J]. Materials Science and Technology, 1997, 13(3): 203 - 209.

[13] 王大勇, 冯吉才, 王攀峰. 搅拌摩擦焊焊热输入数值模型[J]. 焊接学报, 2005, 26(3): 25 - 29.
Wang Dayong, Feng Jicai, Wang Panfeng. Numerical model of heat input from rotational tool during friction stir welding [J]. Transactions of the China Welding Institute, 2005, 26(3): 25 - 29.

作者简介: 姬书得,男,1977 年出生,博士,副教授. 主要从事摩擦焊机理、工艺与仿真方面的研究工作. 发表论文 30 余篇. Email: superjsd@163.com

strengthen the interface by controlling the holding time.

Key words: Ti_3Al-based alloy; transient liquid phase diffusion bonding; interface

Measurement of creep stress exponent of Zn-Al filler metal at room temperature by using nanoindentation JI Feng[1], XUE Songbai[1], LIU Shuang[1], LOU Jiyuan[2], LOU Yinbin[2] (1. College of Materials Science and Technology, Nanjing University of Aeronautics and Astronautics, Nanjing 210016, China; 2. Zhejiang Xinrui Welding Material Co., Ltd, Shaoxing 312400, China). pp 75 - 78

Abstract: The creep behavior of Zn-22Al and Zn-22Al-0.03Ti filler metals at room temperature were studied by nanoindentation in this paper, and constant loading rate method was used to calculate the creep stress exponent. The results indicate that, both the Zn-22Al and Zn-22Al-0.03Ti produced obvious creep deformation under holding load. Both the depth and creep displacement of Zn-22Al-0.03Ti were less than that of Zn-22Al, and the maximum difference were 15.68% and 26.87%, respectively. Under the constant time, the filler metals produced different creep displacement with different loadings. The creep stress exponents of two filler metals at room temperature were obtained by fitting method. Zn-22Al-0.03Ti had a higher creep stress exponent than Zn-22Al filler metal, which implied that Ti-bearing filler metals had better creep resistance than Zn-22Al alloy. The grain of Zn-22Al filler metal could be refined remarkably with the Ti addition, which might result in the increase of grain boundary and finally enhanced the creep resistance of alloy.

Key words: nanoindentation; Zn-Al filler metal; creep; creep stress exponent

Structure and mechanical properties on DH40 ship building steel joints by multi-layer and multi-pass welding technology LU Xuedong[1], CEN Yue[2], WANG Huan[2], WU Mingfang[1] (1. Provincial Key Lab of Advanced Welding Technology, Jiangsu University of Science and Technology, Zhenjiang 212003, China; 2. HuDong-ZhongHua Ship Building Company Limited, Shanghai 200129, China). pp 79 - 83

Abstract: The weldability experiments of DH40 ship building steel were carried out by using the flux-cored wire CO_2 gas shielded multi-pass welding technology. The microstructure and mechanical properties of the joint were studied systematically and the impact toughness was discussed, especially the reason why the impact toughness at HAZ of 5 mm from fusion line of weld root decreased greatly. The results showed that the tensile strength of joints is higher than that of the base metal of 575 MPa. All the samples used in the bending test are qualified and meet the plasticity requirement. The brittleness band is easily formed at HAZ, 5 mm from the fusion line at the weld root. The effect of microstructure heredity results in the coarse crystal grain, which is the secondary reason for the impact ductility decreasing, and the basic reason is the formation of a large amount of granular bainite.

Key words: DH40 steel; multi-pass welding technology; mechanical properties; microstructure

Effect of process parameters on mechanical properties of friction stir welded Al-Li alloy lap joints ZHANG Dandan[1], QU Wenqing[1], YIN Na[1], YANG Mucong[2], CHEN Jie[2], MENG Qiang[3], CHAI Peng[3] (1. School of Mechanical Engineering and Automation, Beihang University, Beijing 100191, China; 2. Shanghai Aircraft Manufacturing Co., Ltd, Shanghai 200436, China; 3. National FSW Center, Aeronautical Manufacturing Technology Research Institute, Beijing 100024, China). pp 84 - 88

Abstract: Through analyzing the microstructure and testing mechanical properties of friction stir welded Al-Li alloy lap joints, the effect of FSW welding parameters on the tensile properties of the lap joints was investigated. The results showed that the length of stir pin has significant influence on the tensile properties of lap joints. When the length of pin is changed from 2.8 mm to 2.5 mm, the ultimate strength and elongation of lap joints are obviously improved. Furthermore, the rotation speed / welding speed (η) also affected the performance of joints. When there was a small increasing in η, the tensile properties of lap joints increased accordingly. For the Al-Li alloy lap structure, the optimum tool rotational speed is 800 r/min, welding speed is 200 mm/min and the length of pin is 2.5 mm, the ultimate strength of lap joint reaches 467 MPa, which is equivalent to 94% that of the base metal and the elongation is 3.18%. In addition, the analysis of tensile fracture appearance indicated that the tensile cracks initiate from the location of "Hooking" defect in the advancing side and grow along the HAZ until to the base metal.

Key words: friction stir welding; aluminum-lithium alloy (Al-Li); tensile properties; fracture

Test and analysis of dynamic process for spot welding of multilayer low carbon steel sheets LI Guizhong, DING Jian, QIN Yuchan, WANG Wenquan (School of Materials Science and Engineering, Jilin University, Changchun 130025, China). pp 89 - 92

Abstract: In the spot welding process, the spot-welded joints of multilayer sheets were always available. The variation of the sheet thickness is obvious in the spot welding process, which makes the impedance fluctuation drastic in secondary circuit of welding power transformer. Thus, the spot welding heat also fluctuates evidently. In this case, the nugget quality cannot be guaranteed if welding heat is not regulated effectively in real time. By means of dynamic test and analysis of welding thermal process, the applicability of different monitoring methods was discussed for spot welding of multilayer low carbon steel sheets. The scientific basis therefore can be provided for manufacturing enterprises to select the exact monitoring method and to achieve the effective quality control.

Key words: low carbon steel; multilayer sheets; spot welding; dynamic process; monitoring method selection

Numerical simulation of metal plastic flow in friction stir welding affected by pin shape JI Shude[1], MENG Qingguo[3], SHI Qingyu[2], ZHANG Liguo[1], ZOU Aili[1] (1. Faculty of Aerospace Engineering, Shenyang Aerospace University, Sheny-

ang 110136, China; 2. Department of Mechanical Engineering, Tsinghua University, Beijing 100084, China; 3. Nantong CIMC Tank Equipment Co., Ltd, Nantong 226001, China). pp 93 – 96

Abstract: The finite volume model of friction stir welding was established on basis of the Fluent software, which considered the practical structure of rotational tool and the relation between the material parameters and temperature. The effect of pin structure on material plastic flow behavior was studied by numerical simulation. The results show that the flow velocity of material decreases with the increase of the distance away from the weldment surface and rotational axis of pin. The flow velocity of material inside weldment increased with decreasing of the cone angle of pine or decreasing of the width of screw pitch. As to the pin with left screw whose rotational direction is clockwise, the flow direction of material near pin is downward while the flow direction near the thermal-mechanical affected zone is upward, which is opposite to that of the pin with right screw.

Key words: friction stir welding; flow; pin; numerical simulation

Laser shock processing power supply topology and control

ZHANG Wei[1], QI Bojin[1], XU Haiying[2], ZOU Shikun[2], CHE Zhigang[2], CAO Ziwen[2], LI Renjie[1] (1. School of Mechanical Engineering and Automation, Beihang University, Beijing 100191, China; 2. Beijing Aeronautical Manufacturing Technology Research Institute, Beijing 100024, China). pp 97 – 100

Abstract: IGBT full-bridge inverter circuit was used as the main circuit topology of the intrinsic and amplifier stage xenon lamp drive power supplies in the Nd glass laser. Double-loop negative feedback control circuits, which include current control in inner loop and voltage control in outer loop, were used in xenon lamp drive power supplies to achieve the constant current charging to the energy storage capacitor at the limited voltage. High-voltage pulse trigger circuit can produce peak voltage of 30 kV and make xenon lamp cut down reliably, which is composed of the gas-discharge tubes and high-voltage pulse transformer. Pulsed xenon lamp discharge trigger circuit is proposed to gain a very high peak power in pulse laser output by adjusting Q mode. This laser shock processing power supply was applied to TC4 titanium alloy tungsten inert gas (TIG) welding joints, and the effect is significant.

Key words: pulsed xenon lamp; full-bridge inverter; laser power supply

Development of flux for soldering of 304 stainless steel

GUAN Yongxing[1], XUE Songbai[1], HAN Ruonan[1], HU Yuhua[2] (1. College of Materials Science and Technology, Nanjing University of Aeronautics and Astronautics, Nanjing 210016, China; 2. The 55th Research Institute, China Electronic Technology Group Corporation, Nanjing 210016, China). pp 101 – 104

Abstract: The spreading properties of Sn-Cu-Ni solder on 304 stainless steel sheet were studied by matching different fluxes, and the results indicated that Sn-Cu-Ni solder has excellent spreadability when it is matched with newly developed flux of H36. Its spreading area reaches 109.56 mm^2, which is increased by 249.4%, 239.3% compared with fluxes of H_3PO_4-C_2H_5OH and $ZnCl_2$-NH4Cl, respectively. Results also indicated that the emulsifier 6500 can further improve the spreadability, and the largest spreading area reaches 157.49 mm^2. It was found that, when the optimized flux H36-2 is matched with Sn-Cu-Ni as solder for 304 stainless steels, the mechanical properties of the soldered joints are superior to the existing literature data, the tensile strength and shear strength of the joints reached up to 22.72 MPa and 33.93 MPa, respectively.

Key words: 304 stainless steel; soldering flux; spreading areas; mechanical properties

Microstructure of 254SMO/Q235B dissimilar steel welded joint

WANG Ke[1], ZHENG Zhentai[1], XUE Haitao[1], SONG Hongwei[2] (1. School of Materials Science and Engineering, Hebei University of Technology, Tianjin 300132, China; 2. Qinhuangdao North Metal Hose Co., Ltd, Qinhuangdao 066000, China). pp 105 – 108

Abstract: Manual TIG was used to weld the dissimilar steel 254SMO/Q235B by taking ERNiCrMo-2, ERNiCrMo-3, ERNiCrMo-10 ERNiCrMo-12, ERNiCrMo-13 and ERNiCrMo-14 nickel-based alloy wire as filler metal. After welding, the welded joint microstructures were analyzed by metallurgical microscope, X-ray diffraction, scanning electron microscope and energy disperse spectroscopy. The results show that when the ERNiCrMo-2, ERNiCrMo-3 and ERNiCrMo-14 welding wire are used, a certain number of cracks will appear in weld. The studies indicate that the welding cracks are solidification cracking. The key factor to cause weld cracking is the difference of physical properties of dissimilar steel and impurity segregation. The welds with good appearance and without welding cracks can be obtained by using the other filler metals.

Key words: super austenitic stainless steel; welding of dissimilar steel; hot cracking; microstructure

Research and application of joining technology at nanometer scale

HE Peng, JIAO Zhen, WANG Jun, LIN Tiesong (State Key Laboratory of Advanced Welding and Joining, Harbin Institute of Technology, Harbin 150001, China). pp 109 – 112

Abstract: Nanomaterials have been widely applied due to their unique properties. Joining technology at nanometer scale is gradually developed with the popularity of nanomaterials, which has broad application prospects in the fields of electronics, aerospace, biology, and health care. The microscopic effects of nanomaterials were introduced and the current development of joining technology at nanometer scale were reviewed. Solid state bonding, soldering/brazing and fusion welding were mainly discussed. The differences in some phenomena and physical processes between nanoscale and macroscale were analyzed. In addition, the function of molecular dynamics simulation in nano-joining field was pointed out. At last, the application prospect of joining technology at nanometer scale was presented.

Key words: joining at nanometer scale; nano materials; molecular dynamics simulation